The Journal of Chemical Physics

Vibrational mode-specific polarization effect in circularly polarized stimulated Raman scattering

Cite as: J. Chem. Phys. **157**, 204201 (2022); https://doi.org/10.1063/5.0124727
Submitted: 07 September 2022 • Accepted: 30 October 2022 • Accepted Manuscript Online: 01 November 2022 • Published Online: 22 November 2022

Yuhui Li, Tao Li, Yuanqin Yu, et al.

The Journal of Chemical Physics ARTICLE scitation.org/journal/jcp

Vibrational mode-specific polarization effect in circularly polarized stimulated Raman scattering

Cite as: J. Chem. Phys. 157, 204201 (2022); doi: 10.1063/5.0124727
Submitted: 7 September 2022 • Accepted: 30 October 2022 •
Published Online: 22 November 2022

Yuhui Li,[1] Tao Li,[1] Yuanqin Yu,[1,a)] Jin Sun,[1] Xiaoguo Zhou,[2] Rui Zhang,[1] and Shilin Liu[2,a)]

AFFILIATIONS

[1] Department of Physics, Anhui University, Hefei, Anhui 230601, China
[2] Hefei National Research Center for Physical Sciences at the Microscale, Department of Chemical Physics, University of Science and Technology of China, Hefei Anhui 230026, China

[a)] **Authors to whom correspondence should be addressed:** yyq@ahu.edu.cn and slliu@ustc.edu.cn

ABSTRACT

As one of the popular coherent Raman scattering techniques, stimulated Raman scattering (SRS) has made significant progress in recent years, especially in label-free biological imaging. Polarization provides an additional degree of freedom to manipulate the SRS process. In previous studies, only linearly polarized SRS was fully investigated, in which both pump and Stokes laser fields are linearly polarized. Here, we theoretically analyzed the SRS process excited by two circularly polarized laser fields and then experimentally demonstrated it by taking a spherical symmetric CH_4 molecule as a model system. The experimental results are in good agreement with the theoretical ones. It is shown that circularly polarized SRS (CP-SRS) has unique characteristics different from linear polarization. When the handedness of circular polarization states of two laser fields is the same, CP-SRS further suppresses the depolarized vibrational band while keeping the polarized band almost unaffected. On the other hand, when the handedness is opposite, CP-SRS enhances the depolarized band while suppressing the polarized band. Therefore, the CP-SRS not only allows us to resolve the symmetry of vibrational modes but also can enhance vibrational contrast based on symmetry selectivity by suppressing or enhancing the signal from a specific vibrational mode. These results will have potential applications in improving chemical selectivity and imaging contrast as well as spectral resolution SRS microscopy. In addition, the CP-SRS has the ability to determine the depolarization ratio ρ and identify the overlapping Raman bands.

I. INTRODUCTION

Coherent Raman scattering (CRS) is a nonlinear optical process associated with third-order susceptibilities ($\chi^{(3)}$) of the medium. With the development of advanced laser sources and detectors, CRS has been a well-established tool for the investigation of the interaction between matter and light fields in various research areas.[1–16] Different from spontaneous Raman scattering, in which only one laser beam is used, CRS is driven by two laser beams (pump field ω_p and Stokes field ω_s), whose frequency difference ($\omega_p - \omega_s$) matches the vibrational transition energy of molecules. As a result, much stronger vibrational signals can be achieved compared to conventional spontaneous Raman scattering. Interest in CRS largely comes from these improved sensitivities, allowing the detection of weak Raman signal and fast response of the medium to the light field.

Beyond the sensitivities, CRS offers more detailed control of molecular orientation in terms of light polarizations. This is because the symmetry properties of a molecule are intrinsically related to third-order nonlinear susceptibilities, whose tensor element describes how molecules will respond to incident laser fields, and so can be selectively excited to obtain the information on molecular symmetry through polarization manipulations. From this point of view, the polarization provides an additional degree of freedom to tune the CRS process.

Among the CRS techniques, coherent anti-Stokes Raman scattering (CARS) and stimulated Raman scattering (SRS) are the most widely used ones. In the former, a new wave at anti-Stokes frequency ($2\omega_p - \omega_s$) is generated, whereas in the latter, the energy transfers from the pump field to the Stokes field, leading to the gain of the Stokes beam and loss of the pump beam as well as molecular

population at vibrational excited state. Correspondingly, there are three ways to detect the SRS process:[17] stimulated Raman gain spectroscopy (SRGS), stimulated Raman loss spectroscopy (SRLS), and photoacoustic Raman spectroscopy (PARS).

Compared with SRS, one disadvantage inherent to CARS is that its spectrum is distorted due to the interference of nonresonant background, causing difficulties in spectral interpretation and limits in final detection sensitivity. To suppress the nonresonant background, the polarization-resolved CARS (P-CARS) has been successfully developed.[18] In addition, P-CARS was used to unravel the information on molecular orientation[19] and Raman optical activity (ROA) for chiral molecules,[20] decompose overlapping vibrational bands, and determine the depolarization ratio of molecular vibrations.[21]

The SRS is considered to be superior in maintaining an undistorted spectral shape since it is free of the nonresonant background of third-order susceptibilities, and thus, the spectral shape is the same as the normal Raman lines. Moreover, the SRS signal exhibits a linear dependence on molecular concentration, convenient to conduct quantitative analysis. In addition, there is no phase matching in SRS. These features render SRS a powerful tool in several fields, especially in label-free biological imaging.[22–26]

The growing interest in SRS has brought important progress in the application of polarization-resolved measurements.[27–36] For example, the manipulation of linear polarization states of SRS has allowed a precise determination of the Raman depolarization ratio.[27–29] Recently, the dual-polarization hyperspectral stimulated Raman scattering microscopy was demonstrated to be simultaneously accessible to two polarized Raman images in orthogonal polarization states, with the ability to measure the symmetry of vibrational bonds and to distinguish the overlapped bands.[30] More recently, polarization-sensitive stimulated Raman scattering was used to resolve amphotericin B orientation in Candida membrane from fingerprint C=C stretching vibration.[35]

Compared to CARS, the potential of polarization application of SRS was not fully exploited. For example, there is no report that clearly shows the dependence of SRS intensity on circularly polarized (CP) laser fields, whereas, for CARS, the use of circular polarization has been theoretically and experimentally demonstrated to have the ability to directly image individual symmetry of samples and enhance the contrast from anisotropic samples in recent studies.[37–39] Here, we investigated the SRS process excited by two circularly polarized (CP) laser fields called CP-SRS. To be contrasted, the SRS process excited by two linearly polarized laser fields is also shown. We will first present the principle of CP-SRS and then our experimental demonstrations.

II. THEORY

The third-order nonlinear susceptibility $\chi^{(3)}$ that describes SRS is a four-rank tensor consisting of 81 components, and the third-order nonlinear polarization density P at ω_s is given by[17,40]

$$P_i^{(3)}(\omega_s) \propto \sum_{jkl} \chi_{ijkl}^{(3)}(-\omega_s;\omega_s,-\omega_p,\omega_p)E_j(\omega_s)E_k^*(\omega_p)E_l(\omega_p), \quad (1)$$

where ω_p and ω_s are the frequencies of pump and Stokes laser fields, respectively, $\chi_{ijkl}^{(3)}$ is the tensor element of the third-order nonlinear susceptibilities, $i, j, k, l = 1, 2, 3$ represents the Cartesian coordinates x, y, z, and * denotes the complex conjugation of incident laser field E. The summation runs over all permutations.

To be contrasted, we first discuss linearly polarized SRS. Briefly, consider that both pump and Stokes beams propagate along the z axis. The Stokes beam is linearly polarized along the x axis, while the pump beam is linearly polarized at an angle of θ relative to the Stokes beam (x axis), as illustrated in Fig. 1(a). Then, the laser fields can be written as

$$\vec{E}(\omega_s) = E_x(\omega_s)\vec{e}_x = E(\omega_s)\vec{e}_x, \quad (2a)$$

$$\vec{E}(\omega_p) = E_x(\omega_p)\vec{e}_x + E_y(\omega_p)\vec{e}_y,$$

$$= E(\omega_p)\cos\theta\vec{e}_x + E(\omega_p)\sin\theta\vec{e}_y, \quad (2b)$$

where $\boldsymbol{e}_x$ and $\boldsymbol{e}_y$ represent the unit vectors of the x and y axes, respectively.

For isotropic medium, carrying out the tensor field product in Eq. (1), the induced polarization density at the x direction becomes

$$\begin{aligned} P_x^{(3)}(\omega_s) \propto\ & \chi_{1111}^{(3)}E_x(\omega_s)E_x^*(\omega_p)E_x(\omega_p) \\ & + \chi_{1122}^{(3)}E_x(\omega_s)E_y^*(\omega_p)E_y(\omega_p) \\ & + \chi_{1221}^{(3)}E_y(\omega_s)E_y^*(\omega_p)E_x(\omega_p) \\ & + \chi_{1212}^{(3)}E_y(\omega_s)E_x^*(\omega_p)E_y(\omega_p), \end{aligned}$$

$$= \left(\chi_{1111}^{(3)}\cos^2\theta + \chi_{1122}^{(3)}\sin^2\theta\right)E(\omega_s)[E(\omega_p)]^2, \quad (3)$$

in which the tensor elements of $\chi_{1221}^{(3)}$ and $\chi_{1212}^{(3)}$ were eliminated due to $E_y(\omega_s) = 0$. It should be mentioned that the SRS is a coherent process in which the induced photons are generated due to seeded photons, and then, all the behaviors of induced photons are the same as the seeded photons, including their frequency, polarization state, and phase. Therefore, for linearly polarized SRS shown in Fig. 1(a), we only need to consider the induced polarization density along the x axis.

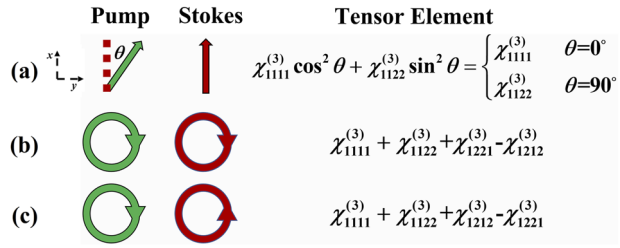

FIG. 1. Polarization configurations of pump and Stokes fields in SRS. (a) Linear polarization, where θ is the cross angle between the linear polarization state of two laser fields. (b) Circular polarization of two laser fields in the same handedness. (c) Circular polarization of two laser fields in the opposite handedness. The tensor elements of $\chi^{(3)}$ involved in each polarization configuration are also shown.

If the light fields are quasi-monochromatic waves along the z direction, the coupled wave equation under slowly varying envelope approximation (SVEA) can be expressed as[17]

$$\frac{\partial E(\omega_s)}{\partial z} = i\frac{\omega_s}{n_s}\sqrt{\frac{\mu_0}{\varepsilon_0}}P_x^{(3)}(\omega_s), \tag{4}$$

where n_s is the refractive index of Stokes beam, and μ_0 and ε_0 are the vacuum permeability and the dielectric constant, respectively. Then, the signal field at the propagation distance L becomes

$$E(\omega_s, L) = \exp\left\{i\frac{\omega_s}{n_s}\sqrt{\frac{\mu_0}{\varepsilon_0}}\left(\chi_{1111}^{(3)}\cos^2\theta + \chi_{1122}^{(3)}\sin^2\theta\right) \times (E(\omega_p))^2 L\right\}E(\omega_s, 0), \tag{5}$$

where $E(\omega_s,0)$ is the initial Stokes field, and L is the interaction length between the pump and Stokes fields. It is known that the third-order nonlinear susceptibility contains the contribution of both resonant and nonresonant parts, i.e.,

$$\chi^{(3)} = \chi_{NR}^{(3)} + \chi_R^{(3)} = \chi_{NR}^{(3)} + \frac{N\sigma}{\omega_R - (\omega_p - \omega_s) - i\Gamma_R}, \tag{6}$$

where Γ_R is the linewidth (HWHM) of Raman resonance corresponding to vibrational frequency, ω_R, N is the molecular number density, and σ is the Raman scattering cross-section. Then, the signal intensity,

$$I(\omega_s, L) = \exp\left\{-\frac{2\omega_s}{n_s}\sqrt{\frac{\mu_0}{\varepsilon_0}}\left(\mathrm{Im}(\chi_{1111}^{(3)})\cos^2\theta + \mathrm{Im}(\chi_{1122}^{(3)})\sin^2\theta\right)I(\omega_p)L\right\}I(\omega_s, 0), \tag{7}$$

where $\mathrm{Im}(\chi^{(3)})$ is the imaginary part of $\chi_R^{(3)}$, and $I(\omega_s, 0)$ is the initial intensity of Stoke field. Under weak signal condition with exponential expansion, the SRS gain can be written as

$$\Delta I(\omega_s) = I(\omega_s, L) - I(\omega_s, 0), \propto \left(\cos^2\theta + \rho\sin^2\theta\right)NL\sigma I(\omega_p)I(\omega_s), \tag{8}$$

where $\mathrm{Im}(\chi_{1111}^{(3)}) \propto \sigma$, and ρ is the Raman depolarization ratio and the relationship of $\rho = \chi_{1122}^R/\chi_{1111}^R$ is applied.[17,40] The proportionality symbol accounts for the omission of some constants, which are the same for linearly and circularly polarized SRS and, thus, do not contribute to the analysis.

For the CP-SRS, we first consider the case that the handedness of circular polarization states of two laser fields is the same, such as right-handedness in Fig. 1(b), and then, the laser fields become

$$\vec{E}(\omega_s) = \frac{1}{\sqrt{2}}E(\omega_s)(\vec{e}_x + i\vec{e}_y), \tag{9a}$$

$$\vec{E}(\omega_p) = \frac{1}{\sqrt{2}}E(\omega_p)(\vec{e}_x + i\vec{e}_y). \tag{9b}$$

Different from linearly polarized SRS, for circularly polarized SRS, the polarization of the initial Stokes field can be projected into any two independent directions, such as the x and y directions in Fig. 1. As a result, the induced polarization density has components at both the x and y polarization directions, and they are

$$P_x^{(3)}(\omega_s) \propto \frac{1}{2\sqrt{2}}\left(\chi_{1111}^{(3)} + \chi_{1122}^{(3)} + \chi_{1221}^{(3)} - \chi_{1212}^{(3)}\right)E(\omega_s)[E(\omega_p)]^2, \tag{10a}$$

$$P_y^{(3)}(\omega_s) \propto \frac{i}{2\sqrt{2}}\left(\chi_{2222}^{(3)} + \chi_{2211}^{(3)} + \chi_{2112}^{(3)} - \chi_{2121}^{(3)}\right)E(\omega_s)[E(\omega_p)]^2. \tag{10b}$$

Using the relationship of $\chi_{1122}^{(3)} = \chi_{1212}^{(3)}$ and $\chi_{1221}^{(3)} = (1-2\rho)\chi_{1111}^{(3)}$[40,41] (Appendix), the SRS gain is (see supplementary material)

$$\Delta I(\omega_s) = \Delta I_x(\omega_s) + \Delta I_y(\omega_s), \propto (1-\rho)NL\sigma I(\omega_p)I(\omega_s), \tag{11}$$

where $\Delta I_x(\omega_s)$ and $\Delta I_y(\omega_s)$ are the components of the CP-SRS gain intensity along the x and y polarization directions, respectively, and $\Delta I(\omega_s)$ is the overall intensity as a sum of them. It should be mentioned that $\Delta I_x(\omega_s)$ and $\Delta I_y(\omega_s)$ are overlapped in space, and they can only be distinguished by adding an extra polarizer before the detector. If no polarizer is added, the overall SRS gain intensity will be detected. In our experiment, the overall gain intensity in CP-SRS was measured.

When the handedness of two circularly polarized fields is opposite, as shown in Fig. 1(c), the induced polarization densities become

$$P_x^{(3)}(\omega_s) \propto \frac{1}{2\sqrt{2}}\left(\chi_{1111}^{(3)} + \chi_{1122}^{(3)} + \chi_{1212}^{(3)} - \chi_{1221}^{(3)}\right)E(\omega_s)[E(\omega_p)]^2, \tag{12a}$$

$$P_y^{(3)}(\omega_s) \propto \frac{i}{2\sqrt{2}}\left(\chi_{2222}^{(3)} + \chi_{2211}^{(3)} + \chi_{2121}^{(3)} - \chi_{2112}^{(3)}\right)E(\omega_s)[E(\omega_p)]^2, \tag{12b}$$

and the gain is (see supplementary material)

$$\Delta I(\omega_s) \propto (2\rho)NL\sigma I(\omega_p)I(\omega_s). \tag{13}$$

From the above analysis, it can be seen that the excitation of a sample with specifically polarized laser fields allows us to probe different components of the susceptibility tensor $\chi^{(3)}$ associated with the SRS process, meaning that the four tensors $\chi_{1111}^{(3)}$, $\chi_{1122}^{(3)}$, $\chi_{1221}^{(3)}$, and $\chi_{1212}^{(3)}$ can be determined by the combinations of linearly polarized and circularly polarized SRS, as summarized in Fig. 1. This is very similar to those demonstrated in another CRS technique, Raman-induced Kerr effect (RIKE).[42–44] In addition to the polarization state of incident laser fields, it can be seen that the SRS intensity is strongly dependent on the depolarization ratio ρ of a specific vibrational mode. For totally symmetric vibrational mode, $0 \le \rho < 3/4$ is called a polarized band. A depolarization ratio of $\rho = 3/4$ is the so-called depolarized band and describes a non-totally symmetric vibration. Therefore, each molecular vibration shows a specific symmetry with a characteristic depolarization ratio ρ.

It should be mentioned that the induced polarization density has a different dependence on tensor elements in CP-SRS given here

and CP-CARS in the literature.[38] This can be understood when considering that the different tensor elements are involved in CARS, SRS, and RIKE even though using the same linear polarization to excite them.[43] In addition, it should be mentioned that the subscript of tensor elements $\chi^{(3)}_{ijkl}$ may be different in the different literature due to the intrinsic permutation symmetry in nonlinear optics,[40,45] which requires that the nonlinear susceptibility be unchanged when simultaneously interchanging two frequency arguments and its two Cartesian indices. For example, in SRS, $\chi^{(3)}_{1122}(-\omega_s;\omega_s,-\omega_p,\omega_p)$ is equivalent to $\chi^{(3)}_{1221}(-\omega_s;\omega_p,-\omega_p,\omega_s)$.

III. EXPERIMENT

The experimental setup is similar to previous studies[27,28] but some modifications were made to measure CP-SRS, as shown in Fig. 2. The laser source is a pulsed Nd: YAG laser (Spectra-physics, 532.1 nm, linewidth 1.0 cm^{-1}, 10 ns, 10 Hz). The output of the YAG laser is divided into two beams. One is used as a pump beam and the other is used to pump a dye laser (ND6000, linewidth 0.05 cm^{-1}) to generate a tunable Stokes beam (624–637 nm). To match the spot size between the pump and Stokes beams, a pair of telescopes is added on the path of the pump beam. Two temporally and spatially overlapped laser beams are focused (f = 35 cm) into the sample cell to generate the SRS process. The SRS signal was detected by the photoacoustic Raman spectroscopy (PARS) technique developed by Barrett and Berry[46] since the SRS process leads to the transfer of ground vibrational state molecules to excited vibrational state. The molecules at the excited vibrational level will relax to the ground state, resulting in a sound wave due to local heat. The sound wave will be detected by a microphone, then amplified to obtain the SRS spectrum. The energies of the pump and Stokes beams are typically 10 and 6 mJ/pulse, respectively. The sample pressure is 5 Torr.

For polarization measurement, the pump and Stokes laser beams were linearly polarized at first, which was achieved by two Glan-Taylor prisms, P_1 and P_2 (extinction ratio $<10^{-6}$). To minimize polarization distortion by the optics, two laser beams were arranged as a counterpropagating configuration.

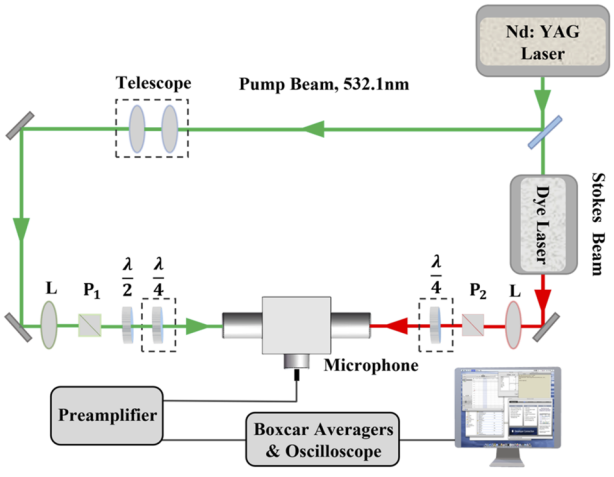

FIG. 2. The experimental setup for linearly and circularly polarized SRS.

When measuring the linearly polarized SRS, the operation in counterpropagation was the same as that in copropagation. The linear polarization of the Stokes beam was fixed in the vertical direction, while that of the pump beam was rotated by a λ/2 wave plate. When measuring CP-SRS, two λ/4 wave plates were added, and the operations between counterpropagation and copropagation were slightly different. For example, to obtain the same handedness of circular polarization state for both pump and Stokes beams, in the counterpropagation, the optical axis of two λ/4 wave plates must be set at a contrary angle (one is 45° and the other is −45°) relative to the polarization direction of pump or Stokes beam, whereas in the copropagation, the optical axis of two λ/4 wave plates must be set at the same angle (45° or −45°). On the contrary, to obtain the opposite handedness of circular polarization, the optical axis of two λ/4 wave plates will be set at the same angle in counterpropagation.

IV. RESULTS AND DISCUSSIONS

To confirm our theory, we have carried out a proof-of-principle experiment on a model system of methane (CH_4). It is known that methane is a highly symmetrical spherical molecule. It has two different C–H stretching vibrational modes, totally symmetric mode υ_1 (2917 cm^{-1}) and nontotally antisymmetric mode υ_3 (3020 cm^{-1}). The depolarization ratios ρ for υ_1 and υ_3 modes are strictly 0 and 3/4 in theory, respectively.

Figure 3 presents the SRS spectra of CH_4 recorded under four different polarization combinations of pump and Stokes fields: (a) parallel linear polarizations, (b) perpendicular linear polarizations, (c) circular polarizations in the same handedness, and (d) circular polarizations in the opposite handedness. From Fig. 3, it can be seen that the SRS intensities change with the changes in polarization states of incident fields. For the polarized υ_1 mode (ρ = 0), the measured intensity ratio is 1:0:0.98:0 in the above four polarization combinations (a)–(d), whereas, for the depolarized υ_3 mode (ρ = 3/4), the intensity ratio is 1:0.76:0.23:1.48. These values are in good agreement with the theoretically predicted intensity ratio at four polarization combinations: 1:0:1:0 for the υ_1 mode and 1:0.75:0.25:1.5 for the υ_3 mode, according to Eqs. (8), (11), and (13). Therefore, the theoretical description of CP-SRS, here, is feasible. In addition, similar to linearly polarized SRS, according to Eqs. (11) and (13), the values of the depolarization ratio of υ_1 and υ_3 modes can be derived from the intensity ratio of CP-SRS at the same and opposite handedness [Figs. 3(c) and 3(d)], and the determined values are 0 and ~0.77 for υ_1 and υ_3 modes, respectively, very close to theoretical values of 0 and 0.75.

Carefully comparing the behaviors of υ_1 and υ_3 modes in linear and circular polarization combinations, it is interesting to find that CP-SRS has its own unique characteristics. This can be explained in the following. On one hand, as shown in Fig. 3(c), when the handedness of circular polarization states is the same, the intensity of the polarized υ_1 mode is almost unchanged compared to parallel linear polarization [Fig. 3(a)], but that of the depolarized υ_3 mode is reduced by ~4 times. However, this reduction is only ~1.33 times in the case of perpendicular linear polarization [Fig. 3(b)], meaning that the CP-SRS in the same handedness has the ability to further suppress the depolarized vibrational mode while keep-

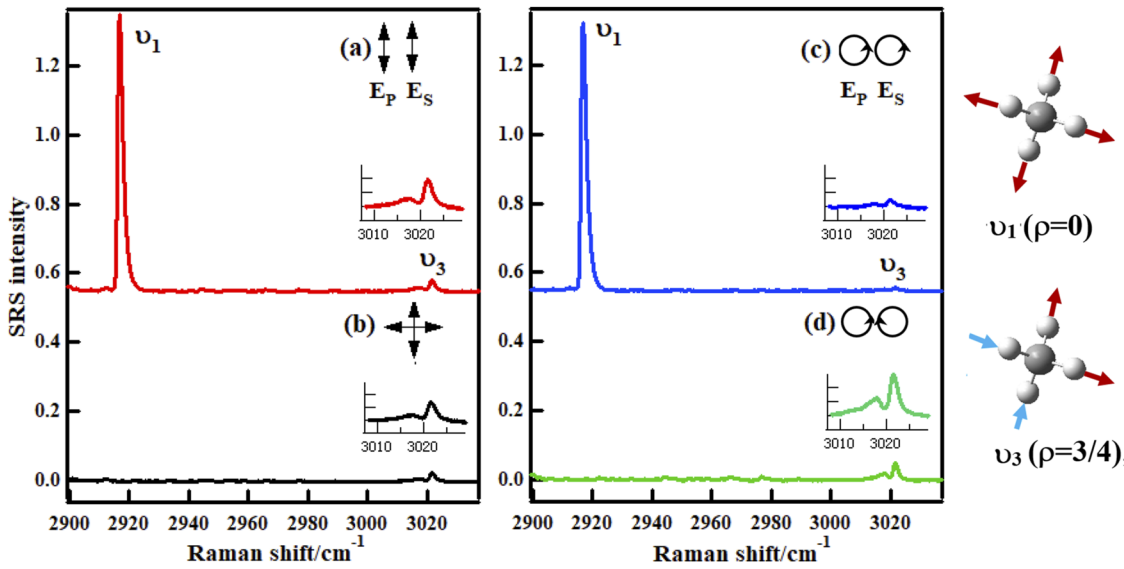

FIG. 3. The SRS spectra of CH_4 molecule in the C–H stretching region. (a) Parallel linear polarizations. (b) Perpendicular linear polarizations. (c) Circular polarizations in the same handedness. (d) Circular polarizations in the opposite handedness. To be clear, the SRS spectrum of υ_3 mode was enlarged and shown in the inset.

ing the polarized mode almost unaffected. On the other hand, as shown in Fig. 3(d), when the handedness of CP-SRS is opposite, the intensity of the polarized υ_1 mode decreases to 0, whereas that of the depolarized υ_3 mode is enhanced by ~1.5 times compared to parallel polarization and ~2 times compared to perpendicular polarization. This indicates that CP-SRS in the opposite handedness has the ability to enhance the depolarized vibrational mode while suppressing the polarized vibrational mode. These characteristics are not shown in linearly polarized SRS.

Therefore, by switching between combinations of left- and right-handed circular polarization states, CP-SRS not only allows us to resolve the symmetry of different vibrational mode but also enhances vibrational contrast based on the symmetry of the Raman mode under study. This contrast capability is very similar to that found by symmetry filtering using circular polarization.[47] From this point, the CP-SRS will open new prospects toward improving chemical selectivity and vibrational contrast as well as spectral resolution in SRS microscopy by suppressing the unwanted vibrational signals.

In addition, CP-SRS makes it easier to distinguish the overlapped Raman peaks. This can be demonstrated in the spectra of cyclohexane (C_6H_{12}) in the C–H stretching region. This molecule is famous for many polarized and depolarized Raman bands. Figure 4 presents the cyclohexane molecule in its chair conformation whose population is about 99% at room temperature. The chair conformation belongs to the D_{3d} point group, in which there are two kinds of different C–H bonds, i.e., axial C–H bond and equatorial C–H bond. Correspondingly, there are two different CH_2 symmetric stretching (SS) modes and two CH_2 antisymmetric stretching (AS) modes due to the vibration from axial and equatorial C–H bonds, respectively. On the other hand, the cyclohexane molecule has two Raman-active CH_2 bending modes in the region of 1400–1500 cm^{-1}. Therefore, the Fermi resonance (FR) can occur between the fundamental of symmetric stretching (SS) and the overtones of bending [called Fermi resonance (FR) modes].

Figure 5 shows the SRS spectra of gaseous cyclohexane in the C–H stretching region recorded under the same four polarization combinations as in Fig. 3. It can be seen that the C–H stretching spectra of cyclohexane are very complex due to spectral overlapping of various bands, including Fermi resonance (FR), CH_2 symmetric stretching (CH_2-SS), and CH_2 antisymmetric stretching (CH_2-AS) in axial and equatorial C–H bonds, as mentioned above. The spectra were assigned by combining with polarization combination measurements and quantum chemistry calculation, and compared with liquid cyclohexane in the literature,[48] as labeled in Fig. 5 and listed in Table S1 in the supplementary material. It can be seen that the separated Raman peaks in Figs. 5(a) and 5(c) are from the polarized SS and FR modes, whereas the broad bands in

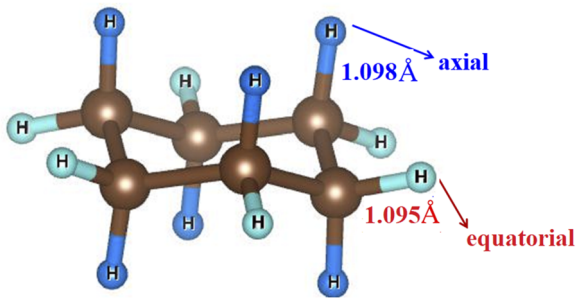

FIG. 4. The geometry of cyclohexane in chair conformation. The dark yellow denotes the C atoms, and the light and dark blue denote the axial and equatorial H atoms, respectively.

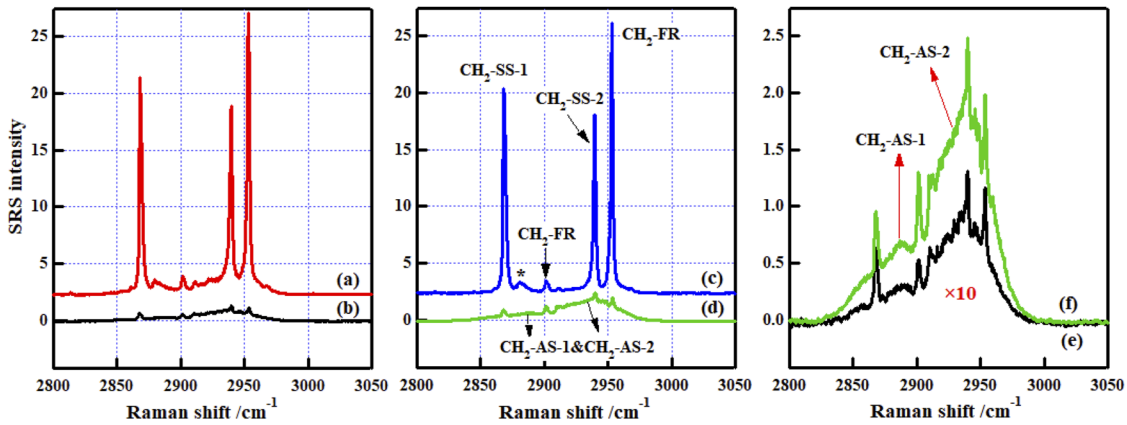

FIG. 5. The SRS spectra of gaseous cyclohexane in the C–H stretching region recorded under four polarization combinations as in Fig. 3. (e) and (f) are the spectra in (b) and (d) enlarged by ten times to be clear, respectively. CH_2-SS-1 and CH_2-SS-2 denote symmetric stretching of axial and equatorial C–H bonds, respectively, and CH_2-AS-1 and CH_2-AS-2 denote the corresponding antisymmetric stretching. FR denotes Fermi resonance mode. * denotes unassigned.

Figs. 5(b) and 5(d) are from the depolarized AS modes. The broadband shape of AS mode is due to the rotational transitions of a depolarized band consisting of all five O, P, Q, R, and S branches in the gas phase, while the polarized band mainly consists of Q branch.

Compared with Fig. 5(a), it is clear that the spectra from the depolarized AS modes are suppressed in Fig. 5(c), leading to the obvious decrease in the broad background from AS modes. On the contrary, compared with weak spectral intensity in Fig. 5(b), the depolarized AS modes are obviously enhanced in Fig. 5(d), further showing that these spectra are from weak CH_2-AS modes and they overlap with strong CH_2-SS and FR modes.

It is known that the depolarization ratio is defined as

$$\rho = \frac{3\gamma^2}{45\alpha^2 + 4\gamma^2}, \tag{14}$$

where α and γ are isotropic and anisotropic invariants that are related to diagonal and off-diagonal elements of the Raman tensor, respectively.[49] For symmetric vibrational mode, the value of ρ is generally close to 0 due to small γ and mainly contributed by isotropic invariant. For antisymmetric mode, the ρ value is totally related to the anisotropic invariant due to $\alpha = 0$. In this sense, the depolarization ratio characterizes the contribution of isotropic and anisotropic vibrations in a Raman mode.

From the above point, CP-SRS may have the potential to highlight anisotropic structures with enhanced vibrational contrast when it is applied to anisotropic samples. Such enhanced vibrational contrast has been recently demonstrated in CP-CARS for anisotropic structures. On the other hand, the use of circular polarization makes SRS independent of the sample orientation, making the contrast enhancement efficient without the need to find an optimal polarization coupling direction relative to the sample. Therefore, the CP-SRS will be suitable for the investigation of anisotropic samples such as crystals and biological samples provided that the laser polarization is less disturbed by samples.

V. CONCLUSION

The use of polarization manipulation offers possibilities for expanding the applications of the SRS technique since the tensor elements of third-order nonlinear susceptibilities $\chi^{(3)}$ describe how the molecules will respond to incident laser fields and so can be selectively excited through polarization combinations. In this work, we theoretically and experimentally demonstrated the SRS process excited by two circularly polarized laser fields. When the handedness of circular polarization states is the same, CP-SRS can further suppress the depolarized vibrational band while keeping the polarized band almost unaffected. When the handedness is opposite, CP-SRS can enhance the depolarized vibrational mode while suppressing the polarized band. These spectral characteristics are significantly different from linearly polarized SRS. The results presented here will open a new window for improving chemical selectivity and imaging contrast as well as spectral resolution in SRS microscopy. Very recently, the CP-SRS microscopy has been developed to increase the epi-detection efficiency of the SRS signal, allowing rapid characterization of bulky brain tissues without tissue pretreatment,[50] but the detailed mechanism of CP-SRS was not discussed there. Our results presented here will provide insight into further interpretation of spectral features in the CP-SRS microscopy. In addition, we know that the chiral molecule has a different response to left-handed and right-handed circularly polarized laser fields, and this is just the principle of Raman optical activity (ROA) spectroscopy. The possibility of CP-SRS application on chiral molecules will be investigated in the future.

SUPPLEMENTARY MATERIAL

The supplementary material provides the evidence for Eqs. (11) and (13) and spectral assignment for cyclohexane in the C–H stretching region.

ACKNOWLEDGMENTS

This work was supported by the National Natural Science Foundation of China (NSFC, Grant Nos. 21873002, 21727804, 21773001, 21873089, and 22073088).

AUTHOR DECLARATIONS

Conflict of Interest

The authors have no conflicts to disclose.

Author Contributions

Yuhui Li: Data curation (equal); Formal analysis (equal); Investigation (equal); Validation (equal); Visualization (equal). **Tao Li**: Data curation (equal); Methodology (equal); Visualization (equal). **Yuanqin Yu**: Conceptualization (equal); Formal analysis (equal); Funding acquisition (equal); Supervision (equal); Writing – original draft (equal); Writing – review & editing (equal). **Jin Sun**: Data curation (equal); Investigation (equal). **Xiaoguo Zhou**: Conceptualization (equal); Funding acquisition (equal); Writing – original draft (supporting). **Rui Zhang**: Writing – review & editing (supporting). **Shilin Liu**: Conceptualization (equal); Funding acquisition (equal); Resources (equal); Writing – review & editing (equal).

DATA AVAILABILITY

The data that support the findings of this study are available within the article and its supplementary material.

APPENDIX: A PROOF OF EQUATION $\chi^{(3)}_{1122} = \chi^{(3)}_{1212}$ and $\chi^{(3)}_{1221} = (1-2\rho)\chi^{(3)}_{1111}$.

In this appendix, we provide a proof of the equation of $\chi^{(3)}_{1122} = \chi^{(3)}_{1212}$ and $\chi^{(3)}_{1221} = (1-2\rho)\chi^{(3)}_{1111}$.

In nonlinear optics, the intrinsic permutation symmetry requires that the nonlinear susceptibility be unchanged when simultaneously interchanging two frequency arguments and its two Cartesian indices.[40] That means for a four-wave mixing process (ω_1, ω_2, ω_3, ω_4),

$$\chi^{(3)}_{ijkl}(\omega_4;\omega_1,\omega_2,\omega_3) = \chi^{(3)}_{ikjl}(\omega_4;\omega_2,\omega_1,\omega_3), \tag{A1}$$

where i, j, k, and l denote the polarization directions (x, y, z) of corresponding light fields.

Similar to the well-known third-order nonlinear optical technique (CARS), the nonlinear refractive index is a four-wave mixing process, as illustrated in Fig. 6.

According to Eq. (A1), for the nonlinear refractive index in Fig. 6,

$$\chi^{(3)}_{ijkl}(-\omega;\omega,\omega,-\omega) = \chi^{(3)}_{ikjl}(-\omega;\omega,\omega,-\omega). \tag{A2}$$

That means

$$\chi^{(3)}_{xxyy}(-\omega;\omega,\omega,-\omega) = \chi^{(3)}_{xyxy}(-\omega;\omega,\omega,-\omega), \tag{A3}$$

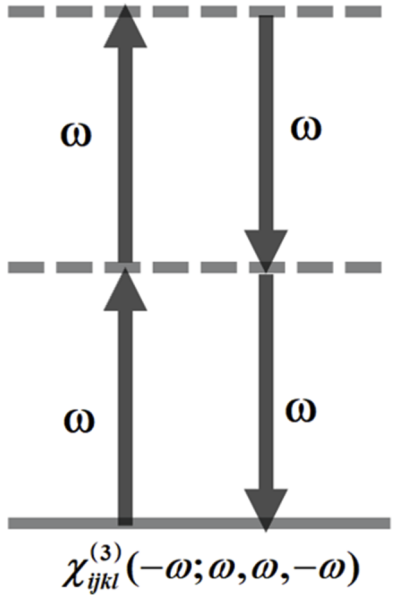

FIG. 6. Energy diagram of nonlinear refractive index effect.

i.e.,

$$\chi^{(3)}_{1122} = \chi^{(3)}_{1212}. \tag{A4}$$

In an isotropic medium, the tensor elements of $\chi^{(3)}$ satisfy the following relationship:

$$\chi^{(3)}_{1111} = \chi^{(3)}_{1122} + \chi^{(3)}_{1212} + \chi^{(3)}_{1221}. \tag{A5}$$

On the other hand, for SRS, the depolarization ratio is defined as[12]

$$\rho = \frac{\chi^{(3)}_{1122}}{\chi^{(3)}_{1111}}. \tag{A6}$$

Then, $\chi^{(3)}_{1122} = \chi^{(3)}_{1212} = \rho\chi^{(3)}_{1111}$, and we have

$$\chi^{(3)}_{1221} = (12\rho)\chi^{(3)}_{1111}. \tag{A7}$$

REFERENCES

[1] C. W. Freudiger, W. Min, B. G. Saar, S. Lu, G. R. Holtom, C. He, J. C. Tsai, J. X. Kang, and X. S. Xie, Science **322**, 1857 (2008).
[2] Y. Li, B. Shen, S. Li, Y. Zhao, J. Qu, and L. Liu, Adv. Biol. **5**, 2000184 (2021).
[3] W.-W. Chen, G. A. Lemieux, C. H. Camp, T.-C. Chang, K. Ashrafi, and M. T. Cicerone, Nat. Chem. Biol. **16**, 1087 (2020).
[4] F. Hu, L. Shi, and W. Min, Nat. Methods **16**, 830 (2019).
[5] C. Zhang and J.-X. Cheng, APL Photonics **3**, 090901 (2018).
[6] H. Rigneault and P. Berto, APL Photonics **3**, 091101 (2018).
[7] D. Polli, V. Kumar, C. M. Valensise, M. Marangoni, and G. Cerullo, Laser Photonics Rev. **12**, 1800020 (2018).
[8] L. Wei, F. Hu, Y. Shen, Z. Chen, Y. Yu, C.-C. Lin, M. C. Wang, and W. Min, Nat. Methods **11**, 410 (2014).

[9]C. H. CampJr., Y. J. Lee, J. M. Heddleston, C. M. Hartshorn, A. R. H. Walker, J. N. Rich, J. D. Lathia, and M. T. Cicerone, Nat. Photonics **8**, 627 (2014).
[10]A. Mandal and L. D. Ziegler, J. Chem. Phys. **155**, 194701 (2021).
[11]S. Oh, C. Lee, W. L. Yang, A. Li, A. Mukherjee, M. Basan, C. Z. Ran, W. Yin, C. J. Tabin, D. Fu, X. S. Xie, and M. W. Kirschner, Proc. Natl. Acad. Sci. U. S. A. **119**, e2117938119 (2022).
[12]J. Ao, Y. Feng, S. Wu, T. Wang, J. Ling, L. Zhang, and M. Ji, Small Methods **4**, 1900600 (2020).
[13]J. Ling, X. Miao, Y. Sun, Y. Feng, L. Zhang, Z. Sun, and M. Ji, ACS Nano **13**, 14033 (2019).
[14]H. Li, Y. Cheng, H. Tang, Y. Bi, Y. Chen, G. Yang, S. Guo, S. Tian, J. Liao, X. Lv, S. Zeng, M. Zhu, C. Xu, J. X. Cheng, and P. Wang, Adv. Sci. **7**, 1903644 (2020).
[15]Z. Liu, W. Su, J. Ao, M. Wang, Q. Jiang, J. He, H. Gao, S. Lei, J. Nie, X. Yan, X. Guo, P. Zhou, H. Hu, and M. Ji, Nat. Commun. **13**, 4050 (2022).
[16]Q. Cheng, L. Wei, Z. Liu, N. Ni, Z. Sang, B. Zhu, W. Xu, M. Chen, Y. Miao, L.-Q. Chen, W. Min, and Y. Yang, Nat. Commun. **9**, 2942 (2018).
[17]G. L. Eesley, *Coherent Raman Spectroscopy* (Pergamon Press, 1981).
[18]J. L. Oudar, R. W. Smith, and Y. R. Shen, Appl. Phys. Lett. **34**, 758 (1979).
[19]J. Duboisset, P. Berto, P. Gasecka, F.-Z. Bioud, P. Ferrand, H. Rigneault, and S. Brasselet, J. Phys. Chem. B **119**, 3242 (2015).
[20]K. Hiramatsu, M. Okuno, H. Kano, P. Leproux, V. Couderc, and H.-o. Hamaguchi, Phys. Rev. Lett. **109**, 083901 (2012).
[21]T. Würthwein, M. Brinkmann, T. Hellwig, and C. Fallnich, J. Chem. Phys. **147**, 194201 (2017).
[22]M. Ji, M. Arbel, L. Zhang, C. W. Freudiger, S. S. Hou, D. Lin, X. Yang, B. J. Bacskai, and X. S. Xie, Sci. Adv. **4**, eaat7715 (2018).
[23]W. J. Tipping, M. Lee, A. Serrels, V. G. Brunton, and A. N. Hulme, Chem. Soc. Rev. **45**, 2075 (2016).
[24]J.-X. Cheng and X. S. Xie, Science **350**, aaa8870 (2015).
[25]C. Zong, R. Premasiri, H. Lin, Y. Huang, C. Zhang, C. Yang, B. Ren, L. D. Ziegler, and J.-X. Cheng, Nat. Commun. **10**, 5318 (2019).
[26]J. Ao, X. Fang, X. Miao, J. Ling, H. Kang, S. Park, C. Wu, and M. Ji, Nat. Commun. **12**, 3089 (2021).
[27]Y. Yu, K. Lin, X. Zhou, H. Wang, S. Liu, and X. Ma, J. Raman Spectrosc. **38**, 1206 (2007).
[28]Y. Yu, K. Lin, X. Zhou, H. Wang, S. Liu, and X. Ma, J. Phys. Chem. C **111**, 8971 (2007).
[29]F. Munhoz, S. Brustlein, R. Hostein, P. Berto, S. Brasselet, and H. Rigneault, J. Raman Spectrosc. **43**, 419 (2012).
[30]J. Shou and Y. Ozeki, Appl. Phys. Lett. **113**, 033701 (2018).
[31]M. Hofer, N. K. Balla, and S. Brasselet, Optica **4**, 795 (2017).
[32]Z. Wang, W. Zheng, C.-Y. S. Hsu, and Z. Huang, Appl. Phys. Lett. **108**, 033701 (2016).
[33]M. Andreana, M.-A. Houle, D. J. Moffatt, A. Ridsdale, E. Buettner, F. Légaré, and A. Stolow, Opt. Express **23**, 28119 (2015).
[34]A. H. Hill, E. Munger, A. T. Francis, B. Manifold, and D. Fu, J. Phys. Chem. B **123**, 8397 (2019).
[35]P.-T. Dong, C. Zong, Z. Dagher, J. Hui, J. Li, Y. Zhan, M. Zhang, M. K. Mansour, and J.-X. Cheng, Sci. Adv. **7**, eabd5230 (2021).
[36]C. M. Valensise, V. Kumar, A. De la Cadena, S. De Silvestri, G. Cerullo, and D. Polli, Opt. Express **27**, 19407 (2019).
[37]C. Cleff, A. Gasecka, P. Ferrand, H. Rigneault, S. Brasselet, and J. Duboisset, Nat. Commun. **7**, 11562 (2016).
[38]P. K. Upputuri, J. Lin, L. Gong, X.-Y. Liu, H. Wang, and Z. Huang, Opt. Lett. **38**, 1262 (2013).
[39]C. Cleff, H. Rigneault, S. Brasselet, and J. Duboisset, Phys. Rev. A **96**, 013851 (2017).
[40]R. W. Boyd, *Nonlinear Optics*, 3rd ed. (Academic Press, New York, 2008).
[41]X.-Q. Yan, X.-L. Zhang, S. Shi, Z.-B. Liu, and J.-G. Tian, Opt. Express **19**, 5559 (2011).
[42]V. Kumar, M. Casella, E. Molotokaite, D. Gatti, P. Kukura, C. Manzoni, D. Polli, M. Marangoni, and G. Cerullo, Phys. Rev. A **86**, 053810 (2012).
[43]C. W. Freudiger, M. B. J. Roeffaers, X. Zhang, B. G. Saar, W. Min, and X. S. Xie, J. Phys. Chem. B **115**, 5574 (2011).
[44]M. O. McAnally, Y. Guo, G. Balakrishnan, G. C. Schatz, and R. P. Van Duyne, Opt. Lett. **41**, 5357 (2016).
[45]Y. R. Shen, *The Principles of Nonlinear Optics* (Wiley, New York, 1984).
[46]J. J. Barrett and M. J. Berry, Appl. Phys. Lett. **34**, 144 (1979).
[47]J. Duboisset, H. Rigneault, and S. Brasselet, Phys. Rev. A **90**, 063827 (2014).
[48]F. A. Miller and H. R. Golob, Spectrochim. Acta **20**, 1517 (1964).
[49]D. A. Long, *The Raman Effect: A Unified Treatment of the Theory of Raman Scattering by Molecules* (John Wiley & Son Ltd., New York, 2002).
[50]K. Bae, W. Zheng, K. Lin, S. W. Lim, Y. K. Chong, C. Tang, N. K. King, C. B. Ti Ang, and Z. Huang, Anal. Chem. **90**, 10249 (2018).